https://doi.org/10.17221/47/2024-SWR

Computed tomographic visualisation and 2D/3D microscopic evaluation of soil macro- and micromorphology

Lubica Pospíšilová[1,3], Jana Plisková[1,6], Victory Armida Janine Jaques[2], Tomáš Zikmund[2], Luboš Sedlák[3], Aleš Eichmeier[4], Aleš Klement[5], Radka Kodešová[5], Luboš Borůvka[5], Jozef Kaiser[2], Ladislav Menšík[6]*

[1]*Department of Agrochemistry, Soil Science, Microbiology and Plant Nutrition, Faculty of AgriSciences, Mendel University in Brno, Brno, Czech Republic*
[2]*CEITEC – Central European Institute of Technology, Brno University of Technology, Brno, Czech Republic*
[3]*Department of Pedology nad Geology, Faculty of Forestry and Wood Technology, Mendel University in Brno, Brno, Czech Republic*
[4]*Mendeleum Institute of Genetics, Faculty of Horticulture, Mendel University in Brno, Lednice, Czech Republic*
[5]*Department of Soil Science and Soil Protection, Faculty of Agrobiology, Food and Natural Sciences, Czech University of Life Sciences Prague, Prague, Czech Republic*
[6]*Division of Crop Management Systems, Crop Research Institute, Prague-Ruzyně, Czech Republic*

**Corresponding author: xplisko2@mendelu.cz*

Citation: Pospíšilová L., Plisková J., Jaques V.A.J., Zikmund T., Sedlák L., Eichmeier A., Klement A., Kodešová R., Borůvka L., Kaiser J., Menšík L. (2024): Computed tomographic visualisation and 2D/3D microscopic evaluation of soil macro- and micromorphology. Soil & Water Res., 19: 176–189.

Abstract: Soil organic matter and pores distribution within aggregates were studied using X-ray computed tomography (XCT; Nikon XT H 225ST and GE Phoenix L240) and advanced 2D/3D measurements by the digital Keyence VHX-6000 microscope (Japan). A new methodological approach with computed tomography involvement for studying the spatial arrangement of pores, porosity, and soil morphology is presented. Changes in studied parameters are documented along the transect of intensively used Haplic Chernozem. Soil disturbance due to erosion and colluvial soil profile formation is reported. Moreover, soil organic matter quality and aggregate stability were evaluated. Obtained results showed statistically significant differences between the control and eroded sites and between eroded and accumulated sites. The correlation coefficients were the highest for soil organic carbon (SOC) and humic substances C_{HS} (r = 0.805) and C_{HS} and C_{HA}/C_{FA} (r = 0.764). The highest porosity, aggregates stability and coefficients stability were confirmed on the eroded site. The computed tomography measurements also document the high disturbance of Haplic Chernozem on the control site and the newly formed profile of Colluvisol. Despite excellent complementary technique further research is necessary to improve micro-XCT resolution and capacity for the soil micromorphological study.

Keywords: aggregate stability; porosity; soil organic matter; X-ray computed tomography

Supported by the projects of MoA QK21010124 „Soil organic matter – indicators of quality", No. FW0601006 „Semi-autonomous system for optimising degraded soils by deep grouting" (MoA, TAČR, Czechia), QK22010251 „Innovation of sorghum management practice for use in ruminant nutrition as an adaptation measure leading to stabilization of forage feed production in the conditions of the changing climate of the Czech Republic", MZE-RO0423, and QK 23020056 "Development and verification of model systems for long-term carbon sequestration in the Czech Republic. This research was also funded by the MEYS from the European Regional Development Fund Project "Centre for the investigation of synthesis and transformation of nutritional substances in the food chain in interaction with potentially harmful substances of anthropogenic origin: comprehensive assessment of soil contamination risks for the quality of agricultural production" (Grant No. CZ.02.1.01/0.0/0.0/16_019/0000845) and CzechNanoLab Research Infrastructure supported by MEYS CR (LM2023051).

https://doi.org/10.17221/47/2024-SWR

The productive potential of any soil depends on morphological characteristics such as structure, texture, consistency, soil depth, and soil chemical properties. Soil texture remains a relatively static soil parameter over a very long period. Most soils exhibit variable soil texture at the topsoil layers with an increasing fineness with depth. On the other hand, soil structure and consistency are highly variable parameters influenced by many factors such as soil biota, organic matter content and quality, mineralogy and iron-rich minerals, moisture, and carbonate content. Both texture and structure determine soil consistency. Soil structure stability and aggregate formation depend on many factors in individual agroecosystems and soil types. The most intensively used soil type in the Czech Republic is Chernozems, which is rich in soil organic matter, and well-structured and medium-textured agricultural soil. However, the distribution and role of a major binding agent (organic matter) is not well understood. Some authors pointed out the crucial role of root-derived organic compounds and earthworm activity in the structure and aggregate formation (Six 1998; Sodhi et al. 2009). Other authors reported a significant role of organic matter in soil aggregability and organo-mineral formation (Six et. al. 2000b, 2004; Fan et al. 2020; Thai et al. 2022). As quoted by Tobiašová (2011), Tobiašová et al. (2018), Weng et al. (2022), Six et al. (2000a), and Six and Paustian (2014) despite the relationship between aggregation stability and organic matter content being widely studied its evaluation is complicated because of many interactions between individual factors and soil parameters). They also showed that structure and aggregate stability are controlled by organic matter content and quality and all these factors are important indicators of soil quality/health. According to them, the increase or decrease of aggregate stability strongly depends also on other soil chemical, biological, and physical properties (e.g. soil reaction, cation exchange capacity, activity and spectrum of soil biota, moisture, temperature etc.). A well-structured soil typically has a mixture of micro-, meso- and macropores and experiences lower soil erosion and higher carbon sequestration (Six et al. 2004, Six & Paustian 2014). Soil aggregates can be classified according to size and shape. Most research is focused on macroaggregates. Unfortunately, different methods for their stability determination are not strongly correlated (Vrána et al. 2024). Usually, the wet sieving method or ultrasound method is used (Le Bissonnais 1996; Pansu & Gautheyrou 2006; Vrána et al. 2024). According to Weng et al. (2022), the soil structure can be in detail study using some new analytical approaches, which can help to visualize the role of organic and inorganic compounds in structure formation. Macro- and micro measurements of aggregates using X-ray computed tomography (XCT) methods can be applied to study agricultural soil disturbance and degradation (Guenat et al. 2019; Pires et al. 2022; Rooney et al. 2022; Ferreira et al. 2023). Guenat et al. (2019) analysed and identified undisturbed zones within a soil monolith to assess the disturbance of agricultural soils in general. They described the spatial arrangement of macropores and presented 3D quantitative measurements of structure elements, particularly pores and pore networks. They could not discriminate between roots and earthworm effects at 1 mm voxel resolution. Higher resolution measurements with 10 um voxel size can help to distinguish casts and macro-aggregates from different worm species. The advantage of the recent advances in imaging methodology and visualization of the root-mediated soil structure in 3D was described by Helliwell et al. (2017). The authors gained a new insight into root-induced physical transformations in the rhizosphere. They aimed at how three different plant species with contrasting root architectures modify the soil structure at the immediate soil surface in comparison with the bulk soil. It was stressed that the root response to the soil was influenced by soil texture (or particle size distribution) and soil type. Finally, they showed that texture, soil compaction, and bulk density affect the root response to soil structuring and using the XCT method can be powerful to observe morphological modification in space. There is also another possibility a 3D observation of soils, using a neutron CT, 4D (time-resolved computed tomography) mostly at the synchrotron sources (Van Veelen et al. 2020; Ferreira et al. 2022). Gerke et al. (2021) worked on chernozem aggregates and focused on the porosity at the nanoscale combining focused ion beam scanning electron microscopy (FIB-SEM) to XCT relatively successfully, while Diel et al. (2019) and Fomin et al. (2023) worked on the impact of wetting/drying cycles on the soil's structure. From the sampling to the 3D object, there are several important steps. Even more so if some quantification needs to be done. Considering the XCT method, there are several important steps from the sampling to the 3D object to beware of, especially concerning minute object visualisation and quantification. After sampling, the sample is scanned by XCT. The projections (radiograms; grey values images based

https://doi.org/10.17221/47/2024-SWR

on material density and X-ray power) of the object are then reconstructed as a 3D volume. Finally, the filtering and segmentation of the object can be done through designed software (VG Studio Max, Avizo, DragonFly, Reactiv'IP, Fiji, and others). One of the key aspects is segmentation as Lavrukhin et al. (2021) explained. They developed neural network segmentation for soils. Other segmentations are available but mostly rely on mature and seedling plants, which is not our case (Mairhofer et al. 2013; Yang 2017). The segmentation relies on the resolution and contrast between the different elements to be analysed in the dataset. Representativity is important and a balance between the sample's size and higher resolution needs to be found. Karsanina et al. (2018) worked on multiscale image fusion, which tackles this problem, even though the process is not straightforward. Karsanina et al. (2018) detailed the importance of the observation scale in soil studies. Carbon storage and interaction between organic and mineral soil phases within aggregate organo-mineral microstructures have not yet been confirmed by direct visualization. There are also many questions about temporal changes in the spatial assemblage of soil organic matter (SOM). This gap and the need to better understand the micro-scale processes of SOM need to be addressed. Our approach employed a combination of standard and advanced 2D/3D measurements such as a digital VHX-6000 microscope (Keyence, Japan), X-ray computed tomography (XT H 225ST, Nikon, Belgium) and GE Phoenix L240 XCT (Universal Systems Inc. USA).

Although many studies exist, organic carbon redistribution and organo-mineral interactions on a microstructure scale have not yet been confirmed by direct visualization. There are also many questions about temporal changes in the spatial assemblage of soil organic matter and a better understanding of SOM processes at the micro-scale need to be addressed.

Chernozems are the most productive and intensively used agricultural soils. Identifying and classifying their disturbance is useful to highlight their further productive potential and pedological development. Due to intensive agriculture two opposite pedogenic processes can be recognized in depleted Chernozems – the colluvial profile formation and Chernozem degradation due to erosion processes. Clarifying these changes on a microscale can give new insight into the soil configuration and improvement of management practices. In this study, we combined standard soil analysis with advanced 2D/3D measurements using a digital Keyence VHX-6000 microscope (Japan), and X-ray micro-computed tomography (XCT). The novelty is to clarify the methodology and identify parameters for disturbed and undisturbed soils using a multi-proxy approach and a combination of different analytical methods.

MATERIAL AND METHODS

Site description. Field experiments were conducted on intensively used arable soil classified as Haplic Chernozems (locality Bošovice, South Moravia, Czech Republic). The climatic area is T2 – warm, and moderately dry. The average rainfall ranges from 500 to 600 mm and the average annual air temperature is 8.8 °C (Quitt 1972; Pospíšilová et al. 2019). The studied area is a part of the Carpathian orogenic system linked to the Eastern Alps. Picha et al. (2006) reported that the Carpathians are divided into two primary domains: The Inner Carpathians deformed and thrust in the Late Jurassic to Early Cretaceous, and the Outer Carpathians deformed and thrust over the European foreland during the Paleogene and Neogene. The Outer Western Carpathians is known as the Carpathian Flysch Belt. In Figure 1 the geological map of the studied area is given. Three soil profile pits were excavated and located by GPS and marked as – the control site, eroded and accumulated sites. The pedogenic horizons and morphological properties such as colour, structure, consistency, mottles, cutans, pores, concretions, horizon boundaries and designation were assessed and described according to procedures outlined in Němeček et al. (2011). Based on the soil survey the soil was classified according to the WRB for Soil Resources (IUSS Working Group WRB 2022) as Haplic Chernozem (Siltic, Epidystric, Ochric) forming on carbonate claystone.

Soil sampling and analysis. The disturbed and undisturbed soil samples were collected from the soil profile at the beginning of the field experiment. Additionally, yearly during the period 2018–2022 grab soil samples after plant harvesting from the topsoil (0–10 cm). A total of 45 punctures in the GPS-localized places from the control, eroded and accumulated sites were analysed yearly (135 disturbed samples in total during the whole experiment period). Undisturbed soil samples were collected from the surface. A total of 45 × 3 undisturbed samples (in 3 repetitions) from GPS points 104, 108, and 114, were examined for physical parameters using physical cores. Commonly used standard analytical methods were applied for their determination (Pansu &

https://doi.org/10.17221/47/2024-SWR

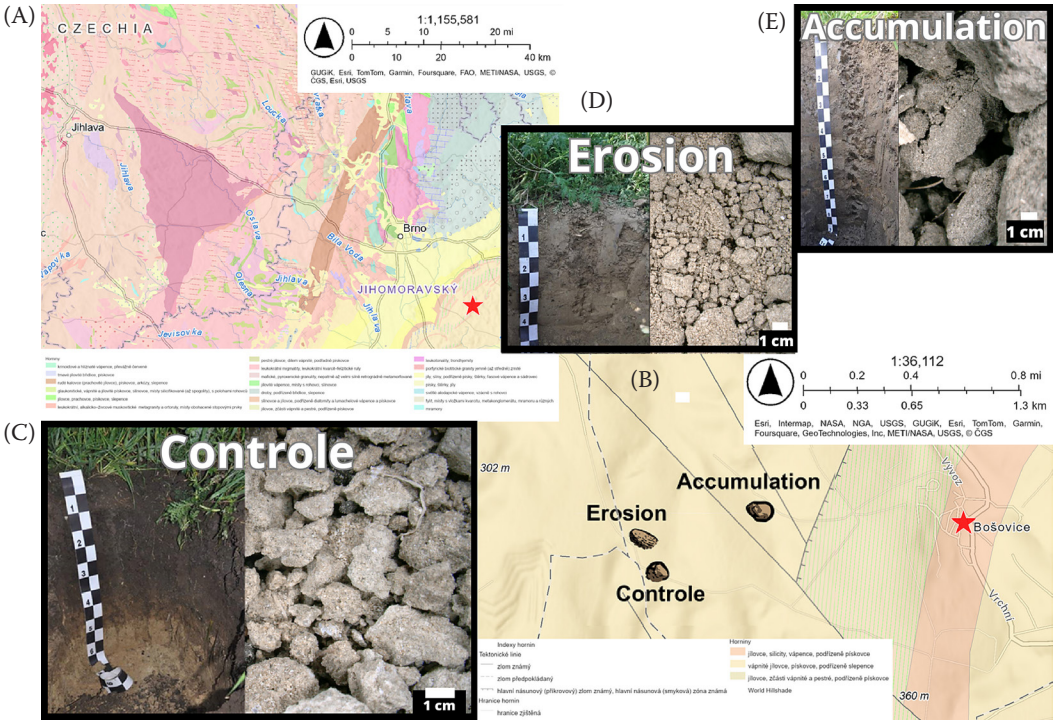

Figure 1. Geological map of Czech Republic (A), map of the sampling sites and soil profiles in different slope positions (B), control site, occupying the top of the hill (C), eroded site, occupying convex slope (D), accumulated site, occupying concave slope (E)

Gautheyrou 2006; Pospíšilová et al. 2019). Disturbed soil samples from each horizon of soil pits and samples from the soil surface were dried at a laboratory temperature of 20 °C and sieved through a 2-mm sieve. Particle size analysis (texture) was determined by the pipette method (Marshall & Holmes 1988). The coefficient of aggregate stability was calculated according to Kandeler (1996). Soil reaction (pH_{H2O}; pH_{KCl}) was measured using pH/conduct-meter (Metrohm, Switzerland). Soil organic carbon (SOC) was determined by wet oxidation in a mixture of sulphuric acid and potassium dichromate (Nelson & Sommers 1996). Fractionation of humic substances was made by a short fractionation method (Kononova & Belčikova 1963). The sum of humic substances ($C_{HS} = C_{HA}/C_{FA}$) was determined by the wet oxidation method, as mentioned earlier. The calculation of the C_{HA}/C_{FA} ratio is reported by Kononova and Belčikova (1963). The C_{HA}/C_{FA} ratio is a widely used criterion for assessing soil quality/health. All soil physical and chemical analyses were done in triplicate. Results were statistically evaluated (ANOVA, Tuckey test) using TIBCO© (Ver. 14.0.0.15, ©1984–2020 TIBCO Software Inc., Palo Alto, CA, USA). Undisturbed soil samples within the soil profile from the control site, eroded, and accumulated sites were examined using advanced 2D/3D measurements and a digital Keyence VHX-6000 microscope (Japan). Additionally, the aggregates' computed tomography (CT) was performed using a Nikon XT H 225ST (Nikon, Belgium). The size of the aggregates varied approximately from one to several centimetres. All aggregates were naturally organized, not sieved or disturbed. Parameters of Nikon XT H 225ST were: beam energy = 100 kV, beam current = 220 µA, power = 22.0 W, effective pixel size = 10.00 µm, exposure total = 2 fps/500 ms, gain = 24 dB, projections = 2 880, frames per projection = 2. After scanning the aggregates, the projection was reconstructed, and the aggregates were cut into 1 836 × 1 836 voxels. Afterwards, all 2D pictures were reconstructed into 3D models (CT Pro 3D 5.3.2, Nikon Metrology) and the model was presented and analysed by voxel analysis software (VG Studio MAX 2023.1, Volume Graphics GmbH). For processing of the aggregate's images, the SoilJ (Koestel 2018) plugin was utilized. We processed the image data using the FIJI distribution of the open-access software ImageJ (Abramoff et al. 2003; Schneider et al. 2012). Its modules automate tasks such as outline recognition, image correction, segmentation, organic

https://doi.org/10.17221/47/2024-SWR

matter and root extraction, and topography detection, as well as morphology and percolation analyses. A total of 17 images (1 836 × 1 836 px) were used from each aggregate for vertical sections and horizontal sections (51 images in total). Three pixels of noise were removed from the images. A GE Phoenix L240 XCT device was used to scan the sample from the Accumulated site (voltage 95 kV; current 210 µA; geometry FDD: 800, FOD: 20; 2 350 projections; voxel size 5 µm). Each set of projections was then subjected to standard tomographic reconstruction procedures. The reconstructed volume was analysed using the commercial software VG Studio Max 3.3 (Volume Graphics; Reinhart (2008)).

RESULTS AND DISCUSSION

Macromorphological features. Macromorphological soil characteristics and analytically determined physical and chemical properties are important for classifying the soil type (Tables 1 and 2). The active soil reaction (pH_{H_2O}) was weakly alkali, the exchangeable soil reaction (pH_{KCl}) was neutral, SOC content was medium or low (due to intensive erosion and management), the stability of aggregates decreased within the soil profile, and the carbonate content varied from 0.5 to 12% and increased with the depth (Table 2). Textural differentiation due to erosion processes affected humus content, structure, consistency, and other chemical and physicochemical parameters of the original soil. The gradual sedimentation and formation of Colluvisol took place in concave slope elements. However, the character of the original parent material (carbonate claystone) was imprinted, on *in-situ* pedogenesis.

In Figure 2 statistically significant differences in studied parameters between the control and erosion sites and eroded and accumulated sites are documented. The correlation coefficients were the highest for SOC and C_{HS} (r = 0.805) and C_{HS} and C_{HA}/C_{FA} (r = 0.764). In addition, the highest values for porosity; aggregates stability and coefficients stability were confirmed on the erosion site and the significant differences between the control and accumulated variants are shown. It was concluded that all studied parameters (BD – bulk density, P – porosity, WSA – water stable aggregates, CAS – coefficient of aggregate stability, SOC – oxidizable carbon,

Table 1. Basic macromorphological description of studied soil profiles

Horizon	Depth (m)	Boundary classes (distinctness, cm)	Texture	Structure	Carbonates (%)	Munsell colour of wet (w) or dry (d) soil sample	Consistency
Control site							
Ap	0–0.35	A	L	G	0.50	7.5YR2/2(w)	FR
ACk	0.35–0.50	C	SL	SAB	I.50	7.5YR3/3(d)	FR
Ck	> 0.50	C	SL	WE	8.00	10YR6/4(d)	FR
Eroded site							
Apk1	0–0.15	A	SL	SAB	12.00	2.5Y6/4(d)	FR
ACk	0.15–0.23	C	L	SAB	12.00	2.5Y7/3.5(d)	FR
Ck	> 0.23	C	SL	WE	12.00	2.5YR7/4(d)	FR
Accumulated site							
A1	0–0.10	C	L	CR	10.00	10YR4/3(w)	FR
A2	0.10–0.20	C	L	CR	IX.80	10YR3/4(w)	FR
A3	0.20–0.30	C	L	CR	10.00	10YR3/4(w)	FR
A4	0.30–0.40	C	L	SAB	X.40	10YR4/4(w)	FM
A5	0.40–0.50	C	L	SAB	X.60	10YR4/3(w)	FM
A6	0.50–0.60	C	L	SAB	X.80	10YR4/3(w)	FM
A7	0.60–0.70	C	L	SAB	X.70	10YR4/3(w)	FM
A8	0.70–0.80	C	L	WE	9.00	2.5Y3/1(w)	SC
A9	0.80–0.90	C	L	WE	9.00	2.5Y3/3(w)	SC

A – abrupt; C – clear; L – loam; SL – silty loam; G – granular; CR–crumbly; SAB – subangular blocky; WE – weak; FR – friable; FM– firm; SC – sticky

https://doi.org/10.17221/47/2024-SWR

Table 2. Average values of selected chemical and physical parameters in studied soil profiles

Horizon	Depth (m)	pH_{H_2O}	pH_{KCl}	SOC (%)	CAS	Texture classes (%)		
						sand 2.00–0.05 mm	silt 0.05–0.002 mm	clay < 0.002 mm
Control site								
Ap	0–0.35	7.60	7.00	1.35	1.83	31.44	37.28	31.28
ACk	0.35–0.50	7.55	7.00	0.60	1.50	41.92	28.80	29.28
Ck	> 0.50	7.70	7.00	0.40	1.40	28.60	45.12	26.28
Eroded site								
Apk1	0–0.15	7.60	7.30	1.10	2.97	37.64	39.64	22.72
ACk	0.15–0.23	7.60	7.20	0.70	2.47	38.72	45.94	15.34
Ck	> 0.23	7.70	7.20	0.30	2.45	38.76	41.00	20.24
Accumulated site								
A1	0–0.10	7.60	7.10	1.10	2.56	27,72	47.36	24.92
A2	0.10–0.20	7.50	7.00	1.10	2.51	29.52	45.68	24.80
A3	0.20–0.30	7.50	7.10	0.74	2.49	34.00	41.72	24.28
A4	0.30–0.40	7.50	7.20	0.60	1.40	34.40	40.68	24.92
A5	0.40–0.50	7.55	7.10	0.45	1.40	41.24	36.60	22.16
A6	0.50–0.60	7.60	7.15	0.41	1.56	37.44	42.76	19.80
A7	0.60–0.70	7.50	7.10	0.33	1.50	32.32	46.40	21.28
A8	0.70–0.80	7.50	7.00	0.42	nd	37.36	27.96	34.68
A9	0.80–0.90	7.60	7.20	0.35	nd	28.16	43.72	28.12

H_2O – distilled water; SOC – soil organic carbon; CAS – coefficient of aggregate stability; nd – not determined

C_{HS} – humic substances, and C_{HA}/C_{FA} ratio) significantly differed on the control, eroded, and accumulated sites. For three parameters (CAS, SOC, C_{HA}/C_{FA}) was also found a statistically significant difference between the control and accumulated sites (Figure 2).

Keyence VHX-6000 micromorphological features. Keyence VHX-6000 2D/3D microscopic measurements illustrated the distribution of SOM and pores in aggregates and helped to choose the proper samples for computed tomography measurements. A combination of different techniques can also provide detailed insight into pores structure on different magnification level. The selected aggregates from the control site (GPS = 104), eroded (GPS = 108) and accumulated sites (GPS = 114) showed that studied sites varied in macro- and micromorphological properties (Figure 3). The control site, Ap horizon (0–0.20 m) was loamy textured, colour 7.5YR 2/2 (wet), friable consistency, a visible mixture of subangular blocky and crumbly structured aggregates, with medium roots content, many worm cats, and many hard carbonate claystone grains and silty clay infilling, well visible organic coating, and also black organic filling inside macropores (Figure 3A). The transition horizon (Ac/Ck horizon; 0.35–0.50 m) was silty loam textured, with a mixture of granularly and subangular blocky structured aggregates, colour 7.5YR 3/3 (dry), with few roots, depleted matrix with no organic coating of aggregates, only several black organic filling inside channels, rich in carbonate claystone skeleton (Figure 3B). The parent material (Ck horizon; > 0.50 m) consists of carbonate claystone, clay minerals, quartz, and feldspars. The colour 10Y6/4 (dry), unique root, occasional organic coating of aggregates and unique black organic filling (Figure 3C). On the erosion site, Ap horizon (0–0.15 m) was very shallow, silty loam textured, with a mixture of subangular blocky and crumbly structured aggregates, and colour 2.5YR 6/4 (dry), mostly matrix of carbonated claystone, with unique roots, unique black organic coating and filling inside aggregates (Figure 3D). The transition horizon (ACk horizon; 0.15–0.23 m) was very shallow, loamy textured, subangular blocky structured, colour 7.5 YR 7/3.5 (dry), mostly matrix of carbonated claystone, with unique roots, unique black organic coating and filling inside aggregates (Figure 3E). The

https://doi.org/10.17221/47/2024-SWR

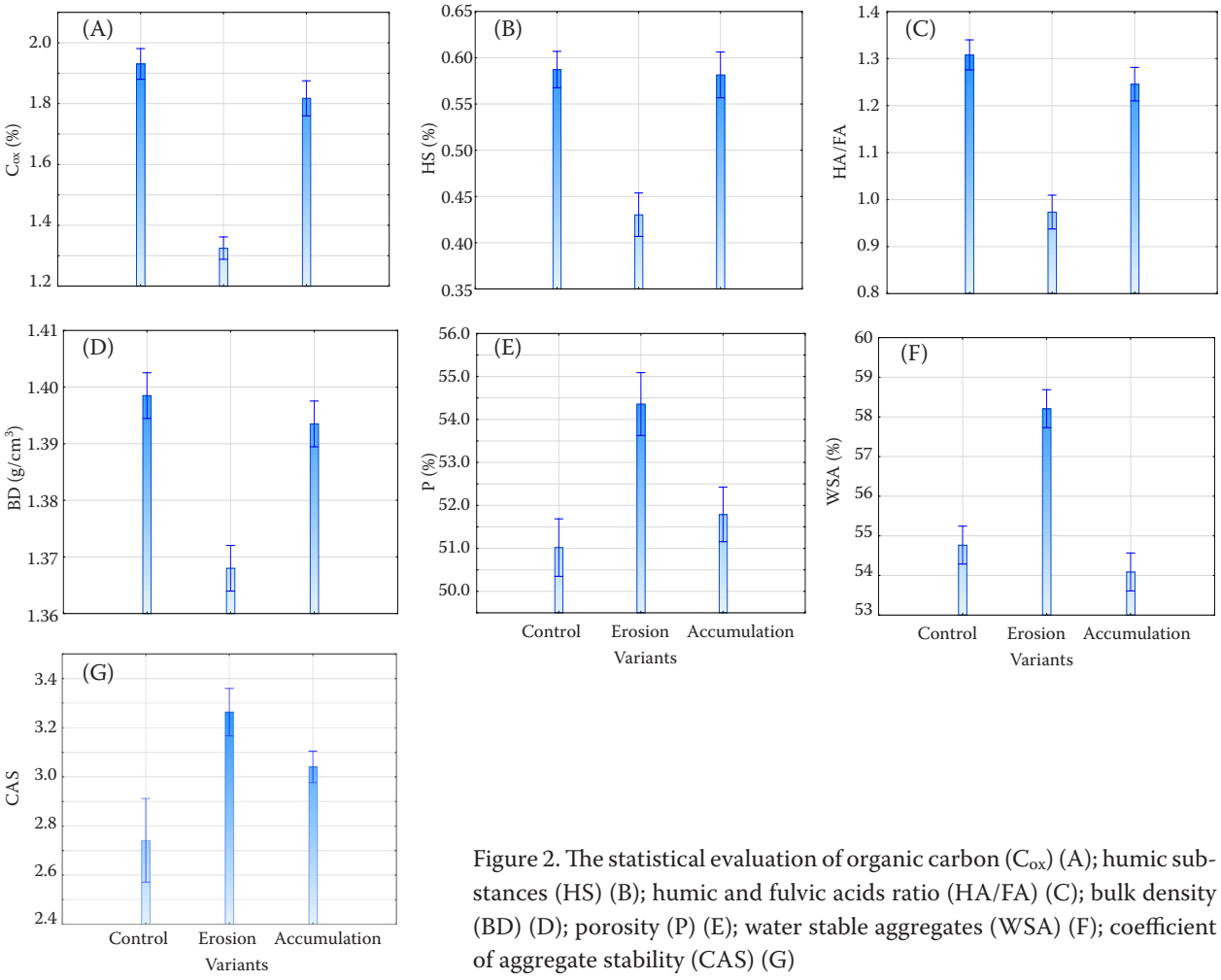

Figure 2. The statistical evaluation of organic carbon (C_{ox}) (A); humic substances (HS) (B); humic and fulvic acids ratio (HA/FA) (C); bulk density (BD) (D); porosity (P) (E); water stable aggregates (WSA) (F); coefficient of aggregate stability (CAS) (G)

parent material (Ck horizon; > 0.23 m) represented by matrix of carbonated claystone, with unique roots, unique black organic coating and filling inside aggregates (Figure 3F). On the accumulation site, the A1 horizon (0–0.10 m) was loamy textured, crumbly structured, colour 10YR 4/3 (wet), friable consistency, with a mixture of subangular blocky and crumbly structured aggregates, rich in black organic coating and black organic filling inside aggregates, medium content of roots, with many worm cats, and carbonate grains (Figure 3G). The A2 horizon (0.10–0.20 m) was loamy textured, crumbly structured, friable consistency, colour 10YR 3/4 (wet), had fewer roots, and a higher content of carbonate claystone skeleton (Figure 3H). The micro photo of the deeper A3 horizon is documented in Figure 3I. The A3, and similarly, A4, A5, A6, and A7 horizons were loamy textured, mostly subangular blocky structured, with friable consistency, similar in colour 10YR 3/4 (wet), unique roots, rich in carbonate claystone skeleton and clay minerals, quartz, and feldspars. The A8 and A9 horizons were loamy textured, weakly structured, with sticky consistency, similar in colour 2.5Y3/1 (wet), unique roots, and rich in carbonate claystone skeleton and clay minerals, quartz, and feldspars. Keyence VHX-6000 not only helped to choose the sample for CT but it was helpful in the description of soil micromorphology.

Nikon XT computed tomography. The size and aggregates variability were in detail studied using computed tomography (CT, Nikon XT H 225ST). The size varied approximately from one to several centimetres. All aggregates were naturally organized, not sieved or disturbed. They were collected from the topsoil on the control site, eroded, and accumulated sites. In Figure 4 aggregates from the control site (2× vertical sections, horizontal section, and overall view).

As mentioned above, a total of 17 images (1 836 × 1 836 px) of each aggregate were studied in vertical

https://doi.org/10.17221/47/2024-SWR

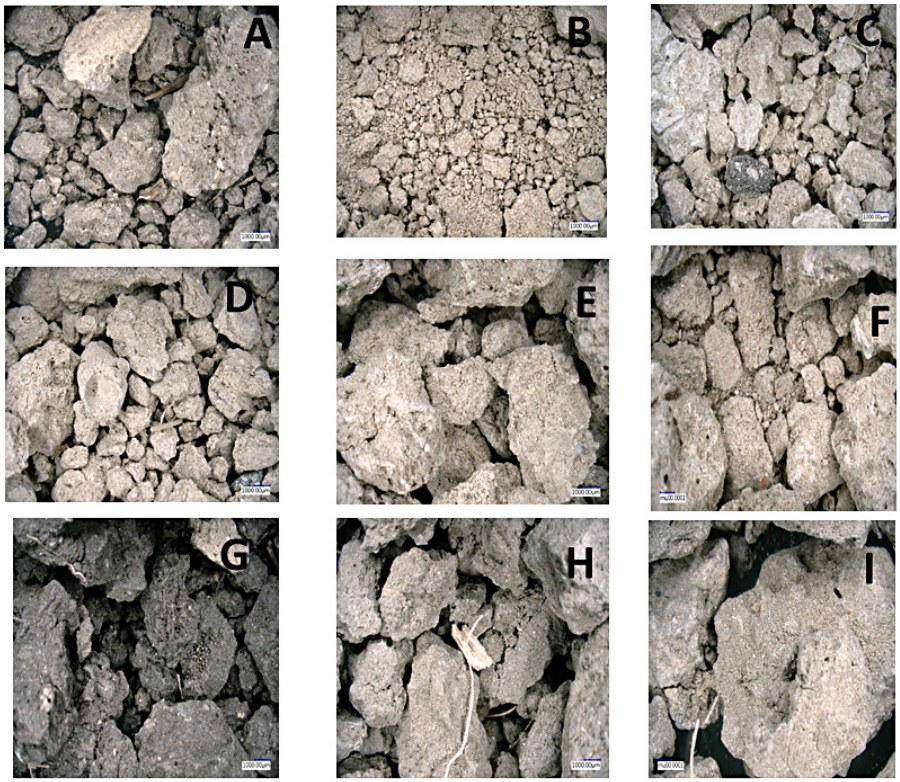

Figure 3. Keyence VHX-6000 micromorphological features within profiles at the control site Ap horizon (A); the control site horizon Ack (B); the control site horizon Ck (C); the eroded site horizon Ap (D); the erosion site horizon Ack (E); the eroded site horizon Ck (F); the accumulation site horizon A1 (G); the accumulation site horizon A2 (H); the accumulation site horizon A3 (I)

sections and horizontal sections (Figure 5). The highest porosity is on the eroded site, followed by the accumulated and control sites. This could be explained by mixing Ap horizon with Ack horizon during the tillage and by the intensive erosion process. According to Keyence VHX-6000 micromorphologi-

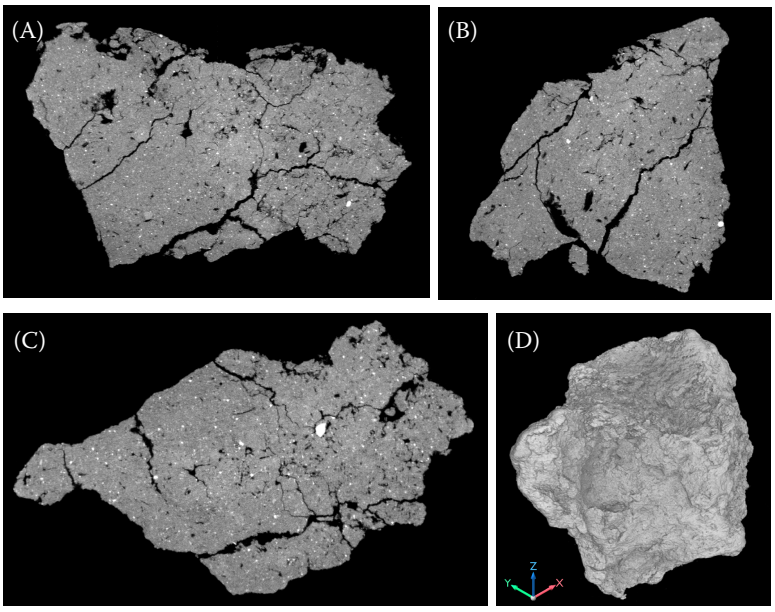

Figure 4. Computed tomography of aggregate AC114: vertical section XY axis (A); vertical section ZY axis (B); horizontal section XZ axis (C); 3D volume of the aggregate AC114 (D)

https://doi.org/10.17221/47/2024-SWR

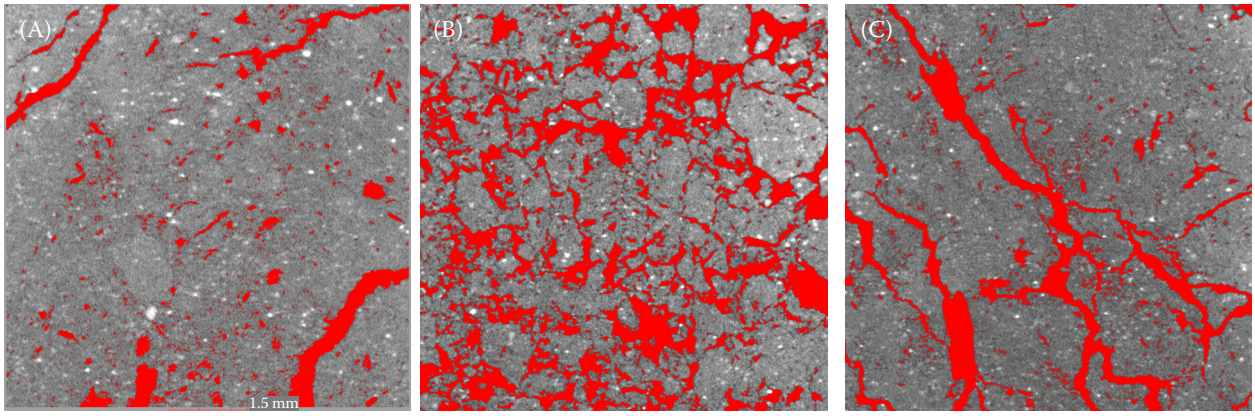

Figure 5. Computed tomography aggregates image with porosity segmentation in red from: the control site (A); the eroded site (B); the accumulated site (C)

cal measurements, the highest organic matter was discovered in the accumulated site (AC_114S Slices XYZ) and in detail studied in 3D mode. The porosity of aggregates was visualized and calculated using computed tomography (Figure 6 and Table 3). The obtained results document that the highest porosity and aggregate stability were on the eroded sites. A higher pores content on the eroded site enhanced water infiltration and drainage making the soil structure more stable. The parent material consisting of the carbonate claystone skeleton is currently used as a ploughing horizon Ap on the eroded site. Additionally, the main conclusion is that also the control site was badly affected by the erosion processes. The total porosity was the lowest (Figure 4 and Table 3). On the accumulated site, medium values of total porosity were achieved. It was concluded that the erosion highly affected aggregate stability and organic

Table 3. Average values of aggregates porosity calculated by computed tomography

Aggregate	Porosity (%)	SD
Control site (102)	8.52	2.80
Eroded site (108)	24.42	1.07
Accumulated site (114)	12.50	1.10
114 – Slices	22.24	0.063

SD – standard deviation

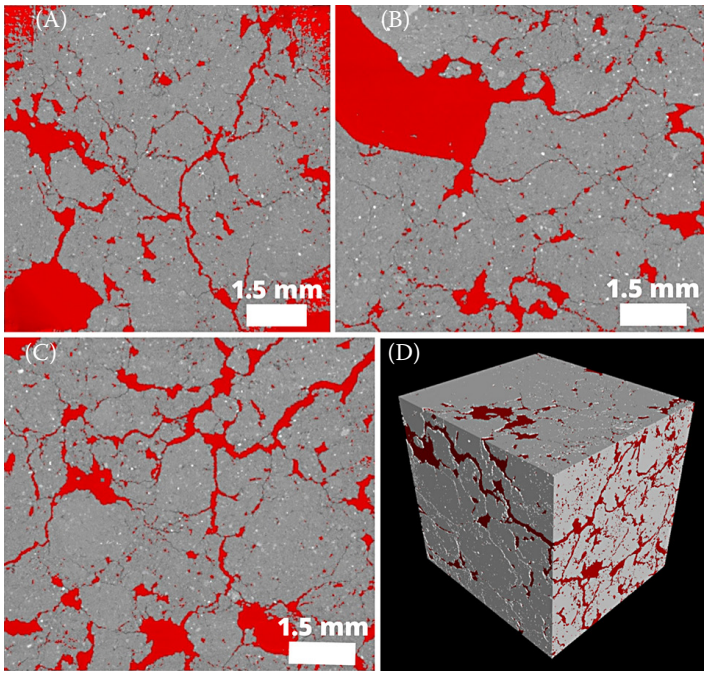

Figure 6. Computed tomography (A, B, C) slices in XY (A), XZ (B), and YZ (C) positions showing the voids and cracks (porosity) in red inside of the matrix; 3D rendering volume of the centre of the aggregate from the accumulated site (AC_114S) showing the porosity in red as well (D)

https://doi.org/10.17221/47/2024-SWR

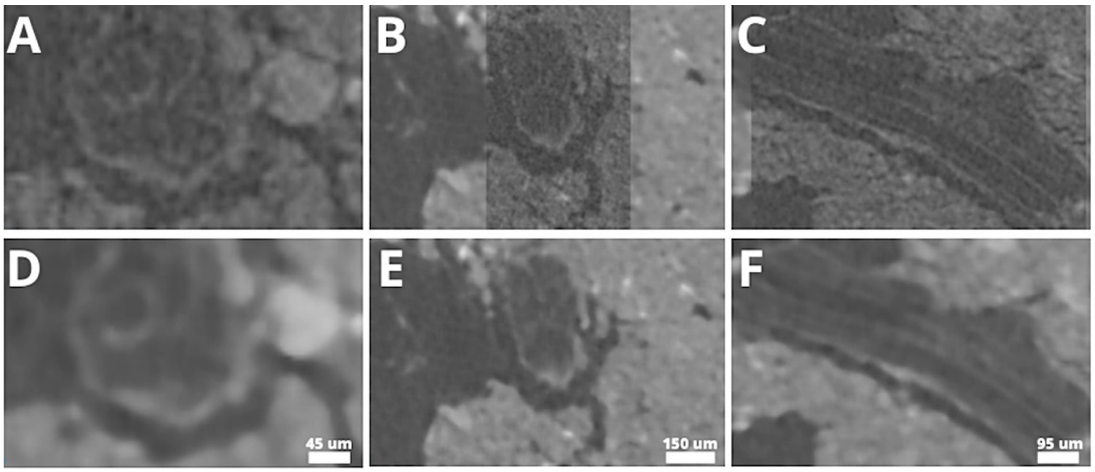

Figure 7. GE Phoenix L240 computed tomography slices in X, Y and Z axis visualization of a twig in the accumulation site aggregate AC_114S: unfiltered images (A–C) and filtered by median 3 px XYZ in VG studio (D–F)
We observe that the filtered slices are blurred, but the general shapes and some lines are more visible than in the unfiltered images (A–C), although some details such as minor cracks and minerals become invisible

matter distribution. Dal Ferro et al. (2013) reported that X-ray micro-CT to evaluate 3D pores is useful for soil quality evaluation. The soil morphological features of undisturbed soil cores and aggregate were a sensitive method for different soil amendments and agricultural practices assessment.

GE Phoenix L240 computed tomography. The focus of these analyses was especially the content, volume, shape, and distribution of soil organic matter in the newly formed colluvial soil profile. We proceeded to an automatic segmentation between materials and background (air) and then separated the inorganic matter from the theoretical organic matter using a grey value threshold. The volume was therefore segmented into 3 components: low, middle, and high attenuation materials. The segmentation not being perfect, and the middle and low-density material overlaps. Manual segmentation would have been needed to correct the segmentation. We used different modules to analyse the materials, such as wall thickness analysis and fibre orientation. The organic material present in the aggregate from the accumulation site (AC_114S) was well visible in the 2D slices of the volume, but their automatic segmentation was hardly possible due to the low contrast between it and the other materials. To improve the visibility of the organic material, the median filter was applied to the dataset. It reduced the noise and offered a higher visualisation of the organic matter borders. Although the image seems partially blurrier, the number of details is still sufficient for organic matter evaluation (Figure 7). The filtered (7A, B, and C) and unfiltered (6D, E, and F) organic twigs were recognised using filtering smooths of the image. The filtered result gives a more blurred image but offers a better visualization of the curves and lines. It also increases the connectivity between the pixels. The general shape of the organic matter is visible but cannot be automatically segmented due to similar attenuation (grey value) of the background and the matrix. One of the aims was to quantify the organic matter in the sample, we tried several operations and analyses to extract only the organic fraction.

Region of interest (ROI) containing part of an organic twig with grey value analysis was observed in the aggregate from the accumulation site (AC 114S) (Figures 8 and 9). This may help to show the areas where organic matter could be. Verifying through the raw grey image slice was always necessary. The separation of the grey values is not optimal for matching with the material, but we observe that the twig is mainly in the light green area even though the grey range goes from 11 760 to 12 560 grey values.

The fibre orientation module was used on a particular ROI of the volume, where we observed root-like shapes. It showed preferential orientation based on the contrasted borders between the root-like and the background, as well as the inorganic matter porosity shape. The extraction of the organic matter can offer a 3D visualization and a preferential view

https://doi.org/10.17221/47/2024-SWR

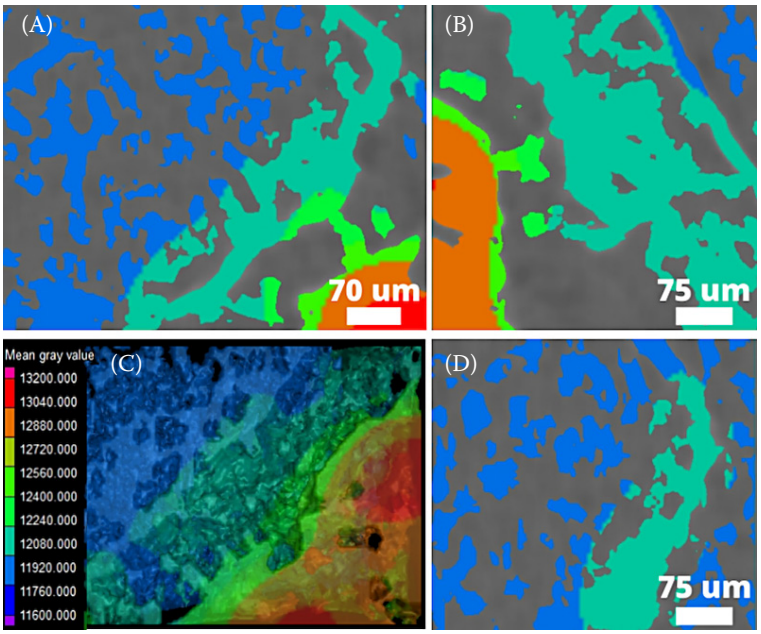

Figure 8. GE Phoenix L240 computed tomography: XYZ axis position slices (A–C) and 3D volume rendering of an organic structure detail showed with grey value (VG studio grey value analysis) in the aggregate from the accumulation site (AC114S) (D) The blue parts reflect low density materials mostly cracks and voids, while the orange-red colours show the higher density material, such as the matrix; the green part reflects the organic matter; as visualized here, it is complicated to discriminate clearly between the different parts and therefore to segment automatically the organic matter directly

of the morphology of a material. We tried several ways to extract the most representative morphology of the aggregate, but due to the low contrast on some parts and the absence of visible material disconnecting partially the shape, it was impossible to extract it with common techniques. We used the wall thickness module to analyse the low attenuation material, which enclosed the organic matter. Several morphological shapes could be determined as organic matter, probably roots and grass residues. We used this module to filter the size range of the material and were able to extract part of a root-like shape. Several morphological operations were applied to this ROI (ROI inversion, filtering, dilation/erosion, mesh transformation) to clean and improve the segmentation of the root-like shape (Figures 8

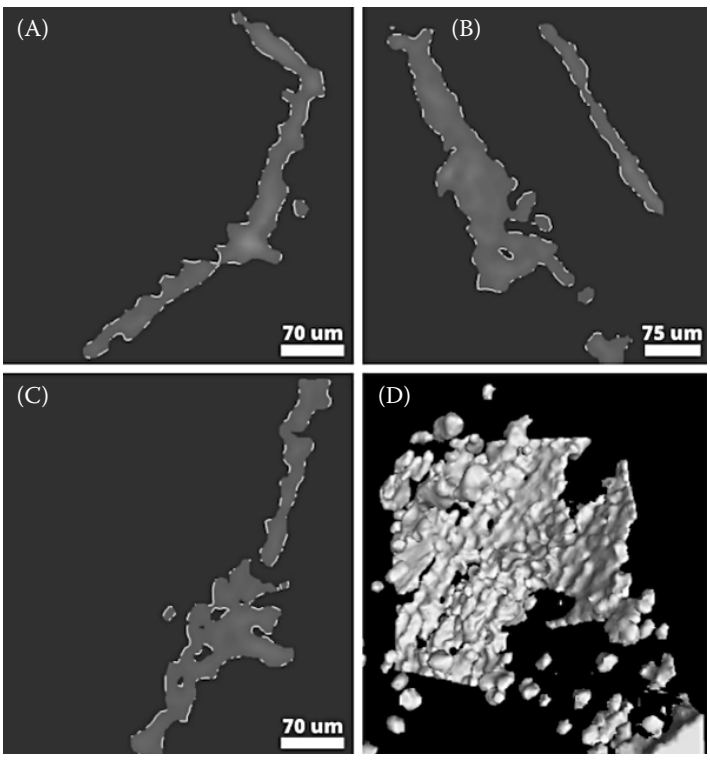

Figure 9. GE Phoenix L240 computed tomography organic matter extraction from the main volume of the accumulation site (AC114S) based on the grey value analysis: XYZ axis position slices of the organic twig (A–C) and 3D volume rendering of the organic structure (D)

https://doi.org/10.17221/47/2024-SWR

and 9). It was observed that the recognised areas are hardly connected. This can be due to the resolution/contrast limit of the device or to the organic matter disaggregation. We observe that even after various enhancement operations and filtering, the whole organic volume could not be extracted from the matrix due to the low contrast between background, matrix and organic matter. The noise is also quite high, which complicates the visualization of the data and its segmentation and if the filtering is increased, the blurring dissolves the grey level of the organic parts hiding some of their details/parts. The roots and twigs can be visually assessed by a human but cannot be automatically retrieved from the volume. Quantitative analyses from the organic matter cannot be used as they are but can give an approximation of the minimum amount present in the aggregate.

The presented results of soil properties on micro- and macroscale, and results of organic matter visualization documented significant differences along the transect (the control, eroded and accumulated sites) and changes within the soil profile. The intense erosion on one side and cumulation of material led to the gradual upbuilding of Colluvisol. The original soil (Haplic Chernozem) rapidly degraded, which was confirmed by organic inhomogeneity, lack of organic coatings on aggregates and visibly less organic fillings in micro- and macropores on the control. Overall, fewer humic substances and less favourable soil properties and distribution of organic matter on the aggregate surface were inherently heterogeneous on the control site. Possinger et al. (2020) studied the spatial separation of SOM, the organo-organic and organo–mineral interactions and observed disordered SOM accumulation at a very fine scale. They showed that these interactions may be dependent on soil physicochemical properties and the soil mineral matrix composition. Compostella et al. (2013) studied the role of SOM in the aggregation process across widely varying agroecosystems, soil types and environments. They confirmed that the character of parent material is imprinted by SOM redistribution and organo-mineral interactions. This was also confirmed by this research. Zádorová et al. (2023) also presented a comprehensive colluvial soil formation and determined varying degrees of Colluvisol maturity. However, the quantification of erosion is difficult because the soil loss alone is not sufficient to estimate the impact of erosion on soil fertility (Holz & Augustin 2021). On the other side, when SOM is not protected within aggregates (Figure 3), it is considered a labile C pool. Similarly, Lavalle et al. (2020) and Holz and Agustin (2021) showed that strong SOM association with minerals represents a stable soil carbon and SOM undergoes extensive mineral decomposition. Wang and Zhang (2024) summarize the advantages and disadvantages of various methods for pore structure determination. They concluded that CT technology can help in future to predict soil hydraulic properties. Presented research documents that appropriate XCT techniques and devices, which are carefully chosen even quantification parameters and other important information on soil organic matter behaviour can provide. The distinguished features inherited from parent rock and properties of newly formed soils bring the necessity of a multi-proxy approach for soil pedogenesis assessment.

CONCLUSION

Several techniques and morphological operations were applied to assess aggregate stability and visualize pores and SOM distributions. This can advance the soil quality evaluation and the understanding of the 3D soil environment. The GE Phoenix L240 computed tomography and ROI containing part of aggregates from the accumulation site (AC 114S) showed that the visualization of the SOM in the slices XYZ is possible and even determination of the organics could be possible through the porosity and residues morphology. Still, the extraction of it for a 3D visualization and its quantification was not feasible except manually. Further research is necessary to improve micro-XCT techniques, resolution, and capacity. If the XCT techniques and devices are carefully chosen even quantification parameters and other important information on soil organic matter behaviour can be received.

REFERENCES

Abramoff M., Magalhães P., Ram S.J. (2003): Image processing with ImageJ. Biophotonics International, 11: 36–42.

Compostella C., Trombino L., Caccianiga M. (2013): Late Holocene soil evolution and treeline fluctuation in the Northern Apennines. Quaternary International, 298: 46–59.

Dal Ferro N., Charrier P., Morari F. (2013): Dual-scale micro-CT assessment of soil structure in a long-term fertilization experiment. Geoderma, 204–205: 84–93.

Diel J., Vogel H.J., Schlüter S. (2019): Impact of wetting and drying cycles on soil structure dynamics. Geoderma, 345: 63–71.

https://doi.org/10.17221/47/2024-SWR

Fan W., Wu J., Ahmed S., Hu J., Chen X., Li X., Zhu W., Opoku-Kwanowaa Y. (2020): Short-term effects of different straw returning methods on the soil physicochemical properties and quality index in dryland farming in China. Sustainability (Switzerland), 12: 1–12.

Ferreira T.R., Pires F.L., Klus R. (2022): 4D X-ray computed tomography in soil science: An overview and future perspectives at mogno/sirius. Brazilian Journal of Physics, 52: 33.

Ferreira T.R., Archilha N.L., Cássaro F.A.M., Pires L.F. (2023): How can pore characteristics of soil aggregates from contrasting tillage systems affect their intrinsic permeability and hydraulic conductivity? Soil and Tillage Research, 230: 105704.

Fomin D.S., Yudina A.V., Romanenko V., Abrosimov K., Karsanina M.V., Gerke K. (2023): Soil pore structure dynamics under steady-state wetting-drying cycle. Geoderma, 432: 116401.

Gerke K.M., Korostilev E.V., Romanenko K.A., Karsanina M.V. (2021): Going submicron in the precise analysis of soil structure: A FIB-SEM imaging study at nanoscale. Geoderma, 383: 114739.

Guenat C., Schomburg A., Fischer F., Luiset A., Le Bayon C., Turberg P. (2019): Extraction of monoliths in unconsolidated soils. In: 8th Int. Symp. Interactions of Soil Minerals with Organic Components and Microorganisms (ISMOM2019), Seville, June 23–28, 2019: 86–87.

Helliwell J.R., Sturrock C.J., Mairhofer S., Craigon J., Ashton R.W., Miller A.J., Whalley W.R., Mooney S.J. (2017): The emergent rhizosphere: imaging the development of the porous architecture at the root-soil interface. Scientific Reports, 7: 14875.

Holz M., Agustin J. (2021): Erosion effect on soil carbon and nitrogen dynamics on cultivated slopes: A meta-analysis. Geoderma, 397: 115045.

IUSS Working Group WRB (2022): World Reference Base for Soil Resources. International Soil Classification System for Naming Soils and Creating Legends for Soil Maps. 4th Ed. Vienna, IUSS, Austria.

Kandeler E. (1996): Aggregate stability. In: Schinner F., Öhlinger R., Kandeler E., Margesin R. (eds.): Methods in Soil Biology. Berlin, Springer-Verlag: 390–395.

Karsanina M.V., Gerke K.M., Skvortsova E.B., Ivanov A.L., Mallants D. (2018): Enhancing image resolution of soils by stochastic multiscale image fusion. Geoderma, 314: 138–145.

Koestel J. (2018): Soil: An image plugin for the semiautomatic processing of three-dimensional X-ray images of soils. Vadose Zone Journal, 17: 1–7.

Kononova M.M., Belčikova N.P. (1963): Short fractionation method of humic substances determination in mineral soils. In: Kononova M.M. (ed): Soil Organic Matter. Moscow, Moscow State University: 228–234. (in Russian)

Lavallee J.M., Soong J.L., Cotrufo M.F. (2020): Conceptualizing soil organic matter into particulate and mineral-associated forms to address global change in the 21st century. Global Change Biology, 26: 261–273.

Lavrukhin E.V., Konstantin A.N., Marina K.V., Kirill G., Romanenko K.A., Romaanenko K., Abrosimov K. (2021): Assessing the fidelity of neural network-based segmentation of soil XCT images based on pore-scale modelling of saturated flow properties. Soil and Tillage Research, 209: 104942.

Le Bissonnais Y. (1996): Aggregate stability and assessment of soil crustability and erodibility: 1. Theory and methodology. European Journal of Soil Science, 47: 425–437.

Mairhofer S., Zappala S., Tracy S., Sturrock C., Bennett M.J., Mooney S.J., Pridmore T.P. (2013): Recovering complete plant root system architectures from soil via X-ray μ-computed tomography. Plant Methods, 9: 1–7.

Marshall T.J., Holmes J.W. (1988): Soil Physics. 2nd Ed. Cambridge, New York, Port Chester, Melbourne, Sydney: Cambridge University Press.

Nelson D.W., Sommers L.E. (1996): Total carbon, organic carbon and organic matter. In: Sparks D.L., Page A.L., Helmke P.A., Loeppert R.H., Soltanpour P.N., Tabatabai M.A., Johnston C.T., Sumner M.E. (eds.): Methods of Soil Analysis. Part 3. Chemical Methods. Madison, Soil Science Society of America: 961–1110.

Němeček J., Muhlhanselová M., Macků J., Vokoun J., Vavříček D., Novák P. (2011): Taxonomic Soil Classification System of the Czech Republic. 2nd Ed. Prague, Czech University of Agriculture. (in Czech)

Pansu M., Gautheyrou J. (2006): Handbook of Soil Analysis. Mineralogical, Organic and Inorganic Methods. Springer.

Picha F.J., Stráník Z., Krejčí O. (2006): Geology and hydrocarbon resources of the Outer Western Carpathians and their foreland, Czech Republic. In: Golonka J., Picha F.J. (eds.): The Carpathians and Their Foreland: Geology and Hydrocarbon Resources. AAPG Memoir, 84: 49–175.

Pires L.F., Ferreira T.R., Cássaro F.A.M., Cooper H.V., Mooney S.J. (2022): A comparison of the differences in soil structure under long-term conservation agriculture relative to a secondary forest. Agriculture, 12: 1783.

Possinger A.R., Zachman M.J., Enders A., Levin B.D.A., Muller D.A., Kourkoutis L.F., Lehmann J. (2020): Organo-organic and organo-mineral interfaces in soil at the nanometer scale. Nature Communication, 11: 6103.

Pospíšilová L., Vlček V., Lukas V., Šarapatka B., Netopil P., Bednář M., Černohorský J., Badalíková B., Vašinka M. (2019): Pedogeochemical characterization of localities Bošovice, Hrušky, and Zástřizly. Brno. Folia Universitatis

https://doi.org/10.17221/47/2024-SWR

Agriculturae et Silviculturae Mendelianae Brunensis: XII: 69. (in Czech)

Quitt E. (1971): Climatic Regions of Czechoslovakia. Studia Geographica 16. Brno, ČSAV-GU. (in Czech)

Rooney E.C., Bailey V.L., Patel K.F., Dragila M., Battu A.K., Buchko A.C., Gallo A.C., Hatten J., Passinger A.R., Qafoku O., Reno L.R., SanClements M., Varga T., Lybrand R.A. (2022): Soil pore network response to freeze-thaw cycles in permafrost aggregates. Geoderma, 411: 115674.

Schneider C.A., Rasband W.S., Eliceiri K.W. (2012): NIH Image to ImageJ: 25 years of image analysis. Nature Methods, 9: 671–675.

Six J. (1998): Aggregation and soil organic matter accumulation in cultivated and native grassland soils. Soil Science Society of America Journal, 62: 1042–1049.

Six J., Paustian K. (2014): Aggregate-associated soil organic matter as an ecosystem property and a measurement tool. Soil Biology and Biochemistry, 68: A4–A9.

Six J., Elliott, E.T., Paustian K. (2000a): Soil structure and soil organic matter II. A normalized stability index and the effect of mineralogy. Soil Science Society of America Journal, 64: 1042–1049.

Six J., Elliott E.T., Paustian K. (2000b): Soil macroaggregate turnover and microaggregate formation: a mechanism for C sequestration under no-tillage agriculture. Soil Biology and Biochemistry, 32: 2099–2103.

Six J., Bossuyt H., Degryze S., Denef K. (2004): A history of research on the link between (micro)aggregates, soil biota, and soil organic matter dynamics. Soil and Tillage Research, 79: 7–31.

Sodhi N.S., Posa M.R.C., Lee T.M., Bickford D., Koh L.P., Brook B.W. (2009): The state and conservation of Southeast Asian biodiversity. Journal of Biodiversity and Conservation, 19: 317–328.

Thai S., Davídek T., Pavlů L. (2022): Causes clarification of the soil aggregates stability on mulched soil. Soil and Water Research, 17: 91–99.

Tobiašová E. (2011): The effect of organic matter on the structure of soils of different land use. Soil and Tillage Research, 114: 183–192.

Tobiašová E., Barančíková G., Gömöryová E., Dębska B., Banach-Szott M. (2018): Humus substances and soil aggregates in the soils 644 with a different texture. Soil and Water Research, 13: 44–50.

Van Veelen, A., Koebernick, N., Scotson C.S., McKay-Fletcher D., Huthwelker T., Mosselmans T.F.W., Roose T. (2020): Root-induced soil deformation influences Fe, S and P: rhizosphere chemistry investigated using synchr tron XRF and XANES. New Phytologist, 225: 1476–1490.

Vrána M., Kubát J.F., Kavka P., Zumr D. (2024): A laser diffractometry technique for determining the soil water stable aggregates index. Geoderma, 441: 116756.

Wang N., Zhang T. (2024): Soil pore structure and its research methods: A review. Soil and Water Research, 19: 1–24.

Weng Z.H., Johannes Lehmann J., Van Zwieten L., Joseph S., Archanjo B.S., Cowie B., Thomsen L., Tobin M.J., Vongsvivut J., Klein A., Doolette C.L., Hou H., Mueller C.W., Enzo Lombi E., Kopittke P.M. (2022): Probing the nature of soil organic matter. Critical Reviews in Environmental Science and Technology, 52: 4072–4093.

Yang X., Varga T., Lie Ch., Scheibe T.D. (2017): What can we learn from in-soil imaging of a live plant: X-ray computed tomography and 3D numerical simulation of root-soil system. Rhizosphere, 3: 259–262.

Zádorová T., Penížek V., Koubová M., Lisá L., Pavlů L., Tejnecký V., Žížala D., Drábek O., Němeček K., Vaněk A., Kodešová R. (2023): Formation of Colluvisols in different soil regions and slope positions (Czechia): Post-sedimentary pedogenesis in colluvial material. Catena, 229: 107233.

Received: May 13, 2024
Accepted: September 4, 2024
Published online: September 24, 2024